LATTICE DESIGN TO ACHIEVE REVERSIBLE MICROBUNCHING IN A STEADY-STATE MICROBUNCHING (SSMB) STORAGE RING

J. Zhao, Z. Pan, X. Deng, A. Chao, C. Tang*, Tsinghua University, Beijing, China

Abstract

Steady-state microbunching (SSMB) has been proposed as a new light source mechanism to generate high average power coherent radiation in electron storage rings. One approach to achieving SSMB is the reversible microbunching scheme, which introduces a laser-based energy modulation to electron bunches in a localized insertion section to form microbunching, and then uses a subsequent energy demodulation to remove the microbunching and restore the bunches to their nominal state in the storage ring. In this paper, we report a modulation–demodulation lattice design for an SSMB storage ring based on the reversible microbunching approach. By self-consistently accounting for non-ideal effects such as intrabeam scattering (IBS) and higher-order nonlinearities, sub-nanometer longitudinal position deviations of the electrons between the laser modulators can be achieved, ensuring precise cancellation of the energy modulation and maintaining the electron bunches in a steady state, thereby ensuring high average radiation power.

INTRODUCTION

High-average-power extreme ultraviolet (EUV) and even soft X-ray sources are in increasing demand for applications in lithography [1] and scientific research [2]. The steady-state microbunching (SSMB) [3, 4] light source has been proposed to address this need. By combining the high repetition rate of storage rings with the high peak power of coherent radiation, SSMB implements precise longitudinal dynamics manipulation to enable electron bunches to emit coherent radiation with power proportional to the square of the number of electrons on a turn-by-turn basis. This mechanism can achieve high average radiation power across a spectrum spanning from THz to X-rays. Different spectral ranges necessitate varying degrees of precision in longitudinal dynamics manipulation. For the EUV regime, several scenarios have been proposed, including Longitudinal Weak Focusing (LWF) [5, 6], Longitudinal Strong Focusing (LSF) [7], and Generalized Longitudinal Strong Focusing (GLSF) [8, 9]. These schemes utilize the extremely small emittance in a certain dimension of the storage ring to achieve very short bunch lengths. In addition to these longitudinal focusing schemes, another approach to realizing SSMB is the reversible microbunching scheme [10]. To realize SSMB in the EUV regime, we specialize this scheme into the Echo SSMB scheme [10]. This method introduces Echo-Enabled Harmonic Generation (EEHG) [11] in a localized section of the ring to induce microbunching at the radiator for coherent emission. Subsequently, an inverse operation is applied to undo the laser modulation and bunch compression, returning the bunch to its equilibrium state. To maintain the steady state of the storage ring during such reversible operations, the modulation insertion region must be as isochronous as possible. This ensures that the energy spread growth, caused by imperfect modulation cancellation, remains minimal and within the tolerance afforded by radiation damping. In this paper, we present an insertion lattice design with sub-nanometer longitudinal path length deviation precision to meet the requirements of high-average-power EUV radiation in Echo SSMB.

* tang.xuh@tsinghua.edu.cn

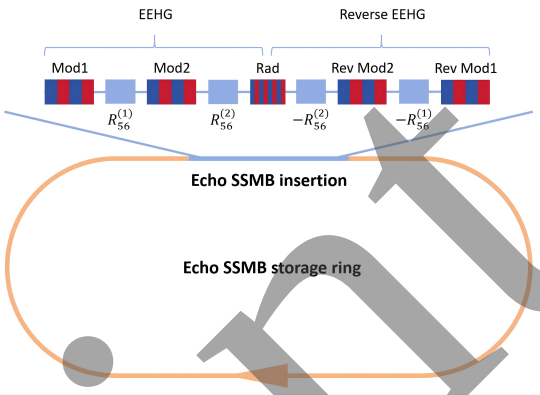

Figure 1: Schematic layout of an Echo SSMB storage ring, highlighting the insertion section encompassing the complete EEHG and reverse EEHG processes.

ECHO SSMB SCHEME

The Echo SSMB storage ring layout is illustrated in Fig. 1. Initially, the modulators Mod1 and Mod2, along with the $R_{56}^{(1)}$ and $R_{56}^{(2)}$ lattices, are configured to generate an optimal bunching factor at the radiator center. To ensure reversibility, a $-R_{56}^{(2)}$ lattice is employed to cancel $R_{56}^{(2)}$, forming an isochronous achromat between Mod2 and Rev Mod2, defined as the inner lattice. Subsequently, the energy modulation from Mod2 is removed by Rev Mod2, and a $-R_{56}^{(1)}$ lattice is introduced to neutralize $R_{56}^{(1)}$, constituting the outer lattice.

The longitudinal dynamics of the insertion are given by

$$\begin{aligned} \delta &= \delta + A_1 \sin(k_L z), \quad z = z + R_{56}^{(1)}\delta; \\ \delta &= \delta + A_2 \sin(k_L z), \quad z = z + R_{56}^{(2)}\delta; \\ z &= z - R_{56}^{(2)}\delta, \quad \delta = \delta - A_2 \sin(k_L z); \\ z &= z - R_{56}^{(1)}\delta, \quad \delta = \delta - A_1 \sin(k_L z), \end{aligned} \tag{1}$$

where A_1 and A_2 are the relative modulation amplitudes. Longitudinal path length deviations between the laser modulators lead to an increase in the energy spread of the storage

ring

$$\Delta\delta = -A\left\{\sin\left[k_L(z+\Delta z)\right] - \sin(k_L z)\right\}. \tag{2}$$

The energy spread growth induced by the longitudinal path length deviations of the inner and outer lattices can be expressed as

$$\begin{aligned}\Delta\sigma^2_{\delta,\text{inner}} &\approx \frac{(A_1 k_R)^2}{4}\sigma^2_{\Delta z,\text{inner}},\\ \Delta\sigma^2_{\delta,\text{outer}} &\approx \frac{(A_1 k_L)^2}{2}\sigma^2_{\Delta z,\text{outer}},\end{aligned} \tag{3}$$

where k_L and k_R are the wavenumbers of the modulation laser and the radiation, respectively. Here, the approximations $R^{(1)}_{56}/R^{(2)}_{56} \approx n$ and $|A_2 k_L R^{(2)}_{56}| \approx 1$ are used. Since $k_R \gg k_L$, the storage ring has a much stricter tolerance for path length deviations in the inner lattice. In the Echo SSMB scenario, the required tolerance for the inner lattice is typically on the sub-nanometer scale.

NONLINEAR PATH LENGTH DEVIATION

Lattice nonlinearities between the laser modulators are a primary source of path length deviations. In the uncorrected case, second-order nonlinearities dominate. Considering an achromat consisting only of horizontal bends without horizontal-vertical coupling, the second-order path length deviation of an electron in the lattice can be expressed as

$$\begin{aligned}\Delta z =& T_{511}x^2 + 2T_{512}xx' + T_{522}x'^2 + T_{533}y^2 + 2T_{534}yy'\\ &+ T_{544}y'^2 + 2T_{561}x\delta + 2T_{562}x'\delta + T_{566}\delta^2,\end{aligned} \tag{4}$$

where x, x', y, y', z, δ are the six-dimensional phase-space coordinates at the lattice entrance, and T_{ijk} represents the second-order Taylor map elements of the lattice. To minimize the energy spread growth, the variance of Δz , denoted as $\sigma_{\Delta z}$, must be optimized. According to Ref. [12], this $\sigma_{\Delta z}$ can be expressed in terms of the emittances, energy spread, and the normal form coefficients of the Hamiltonian

$$\begin{aligned}\sigma^2_{\Delta z} =& 4h^2_{11001}\epsilon_x^2 + 4|h_{20001}|^2\epsilon_x^2 + 4h^2_{00111}\epsilon_y^2\\ &+ 4|h_{00201}|^2\epsilon_y^2 + |h_{10002}|^2\epsilon_x\sigma_\delta^2 + 2h^2_{00003}\sigma_\delta^4.\end{aligned} \tag{5}$$

By considering the phase dependence of the three coefficients

$$\begin{aligned}h_{20001} &\propto \exp(2i\mu_x),\\ h_{00201} &\propto \exp(2i\mu_y),\\ h_{10002} &\propto \exp(i\mu_x),\end{aligned} \tag{6}$$

and employing N lattice cells, each with a transverse betatron phase $\frac{2k\pi}{N}$, where k and N are integers, and ensuring $\frac{k}{N}$ avoids integer and half-integer values, these three terms can be eliminated. This leaves only the horizontal and vertical chromaticities and T_{566}, which can then be perfectly corrected using three sextupole families to achieve full second-order nonlinear cancellation. Any residual third-order nonlinearities can be further corrected using octupoles.

IBS INDUCED PATH LENGTH DEVIATION

When a bunch traverses a lattice section, the energy and momentum kicks induced by the IBS effect are propagated to the downstream laser modulator via the partial R_{56}, R_{51}, and R_{52} terms, transforming into a path length deviation $\sigma_{\Delta z}$ which can be expressed as [13]

$$\begin{aligned}\sigma^2_{\Delta z,\text{IBS}} =& \int_{s_0}^{s_1} R_{56}(s,s_1)^2\frac{\langle\Delta\delta\Delta\delta\rangle}{cdt}ds\\ &+ \int_{s_0}^{s_1} R_{52}(s,s_1)^2\frac{\langle\Delta x'\Delta x'\rangle}{cdt}ds\\ &+ \int_{s_0}^{s_1} 2R_{52}(s,s_1)R_{56}(s,s_1)\frac{\langle\Delta\delta\Delta x'\rangle}{cdt}ds,\end{aligned} \tag{7}$$

where $\frac{\langle\Delta\delta\Delta\delta\rangle}{cdt}$, $\frac{\langle\Delta x'\Delta x'\rangle}{cdt}$, and $\frac{\langle\Delta\delta\Delta x'\rangle}{cdt}$ are the second-order momentum diffusion rates [14] induced by IBS, $R_{ij}(s_1, s)$, representing the lattice transfer matrix elements from s to s_1, and s_0 denotes the starting point of the lattice. The resulting $\sigma_{\Delta z}$ for the inner and outer lattices are denoted as $\sigma_{\Delta z,\text{inner,IBS}}$ and $\sigma_{\Delta z,\text{outer(1),IBS}}$, respectively.

Furthermore, the energy spread growth caused by IBS in the inner lattice also contributes to the $\sigma_{\Delta z}$ of the outer lattice through the $R^{(1)}_{56}$ term

$$\sigma^2_{\Delta z,\text{outer(2),IBS}} \approx (R^{(1)}_{56})^2\int_{\text{inner}}\frac{\langle\Delta\delta\Delta\delta\rangle}{cdt}ds. \tag{8}$$

Consequently, the total energy spread growth induced by IBS is given by

$$\begin{aligned}\Delta\sigma^2_{\delta,\text{IBS}} =& \frac{(A_1 k_R)^2}{4}\sigma^2_{\Delta z,\text{inner,IBS}}\\ &+ \frac{(A_1 k_L)^2}{2}(\sigma^2_{\Delta z,\text{outer(1),IBS}} + \sigma^2_{\Delta z,\text{outer(2),IBS}}).\end{aligned} \tag{9}$$

INNER LATTICE DESIGN

Due to the strict tolerance for the $\sigma_{\Delta z}$ of the inner lattice in the storage ring, a precision lattice design is required. Therefore, we present a lattice design with a $\sigma_{\Delta z}$ on the sub-nanometer scale. The layout, beta functions, and dispersion functions of the inner lattice are shown in Fig. 2.

We employ a three-period lattice and four sextupole families to correct the second-order nonlinearities of the entire inner lattice while simultaneously minimizing sextupole-induced third-order effects. By accounting for the contributions of $\sigma_{\Delta z,\text{inner,IBS}}$ and $\sigma_{\Delta z,\text{outer(2),IBS}}$ to the inner lattice, the IBS-induced $\sigma_{\Delta z}$ is calculated to be 0.354 nm. Based on tracking simulations using ELEGANT [15], octupoles are introduced to correct residual third-order nonlinearities, such as second-order chromaticities and the Q_{5666} term. The resulting path length deviation induced by nonlinearities is reduced to 0.0784 nm for horizontal and vertical emittances of 1 nm and an energy spread of 1.3×10^{-3}.

Figure 3 illustrates the longitudinal phase space of a bunch slice with zero initial bunch length, 1 nm horizontal and vertical emittances, and 1.3×10^{-3} energy spread after traversing

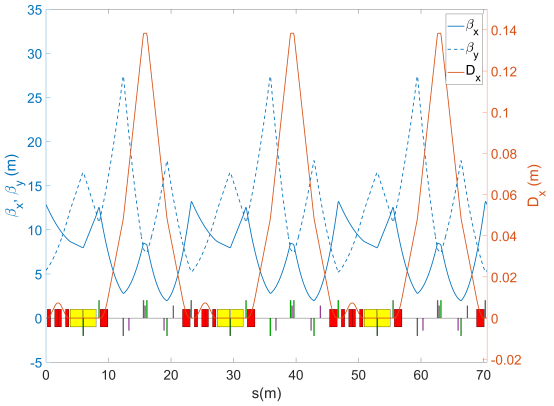

Figure 2: Magnet layout and optical functions of the inner lattice. The horizontal and vertical β functions are represented by blue solid and dashed lines, respectively, while the dispersion function is shown as an orange solid line. The colored rectangles indicate different magnets: dipoles (red), quadrupoles (green), sextupoles (purple), and undulators (yellow).

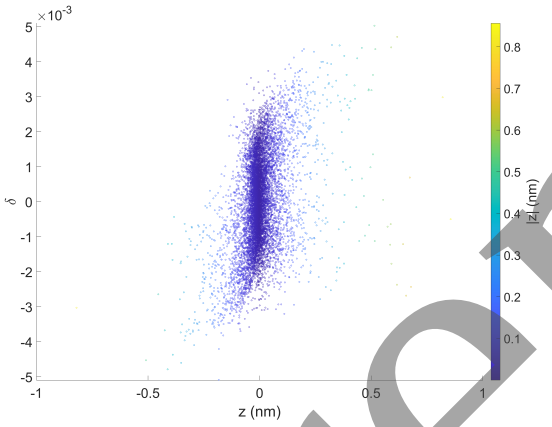

Figure 3: Longitudinal phase space of the bunch slice. The color scale indicates the absolute longitudinal position $|z|$ in nanometers.

this lattice. This result demonstrates excellent nonlinear isochronicity. The total equivalent path length deviation of the entire inner lattice is 0.363 nm, which is well within the acceptable tolerance for the Echo SSMB storage ring.

CONCLUSION

In this paper, we analyze the primary sources of path length deviation in the insertion of an Echo SSMB storage ring, specifically focusing on lattice nonlinearities and IBS. For second-order nonlinearities, we demonstrate that specific linear lattice designs can be utilized to achieve effective cancellation and perfect correction. By further accounting for higher-order nonlinearities and IBS effects, we propose a design for the inner lattice, the most sensitive section with the strictest tolerance, that achieves a longitudinal path length deviation of $\sigma_{\Delta z} = 0.363\,\text{nm}$. This sub-nanometer precision lattice provides a robust foundation for maintaining the steady state of an Echo SSMB storage ring.

REFERENCES

[1] D. Kazazis, J. G. Santaclara, J. van Schoot, I. Mochi, and Y. Ekinci, "Extreme ultraviolet lithography", *Nat. Rev. Methods Primers*, vol. 4, p. 84, 2024. doi:10.1038/s43586-024-00361-z

[2] B. Lv, T. Qian, and H. Ding, "Angle-resolved photoemission spectroscopy and its application to topological materials", *Nat. Rev. Phys.*, vol. 1, pp. 609–626, 2019. doi:10.1038/s42254-019-0088-5

[3] D. Ratner and A. Chao, "Steady-state microbunching in a storage ring for generating coherent radiation", *Phys. Rev. Lett.*, vol. 105, p. 154801, 2010. doi:10.1103/PhysRevLett.105.154801

[4] A. Chao, E. Granados, X. Huang, D. F. Ratner, and H. W. Luo, "High Power Radiation Sources using the Steady-state Microbunching Mechanism", in *Proc. IPAC'16*, Busan, Korea, May 2016, pp. 1048–1053. doi:10.18429/JACoW-IPAC2016-TUXB01

[5] X. Deng, *Theoretical and experimental studies on steady-state microbunching*. Springer Nature, 2024.

[6] Z. Pan, "Research on optimization and design of advanced laser-driving storage ring", Ph.D. thesis, Tsinghua University, 2020.

[7] Y. Zhang, "Research on longitudinal strong focusing SSMB ring", Ph.D. thesis, Tsinghua University, 2022.

[8] Z. Li, X. Deng, Z. Pan, C. Tang, and A. Chao, "Generalized longitudinal strong focusing in a steady-state microbunching storage ring", *Phys. Rev. Accel. Beams*, vol. 26, p. 110701, 2023. doi:10.1103/PhysRevAccelBeams.26.110701

[9] X. Deng, A. Chao, W. Huang, Z. Li, Z. Pan, and C. Tang, "Steady-state microbunching based on transverse-longitudinal coupling", *Nucl. Sci. Tech.*, vol. 37, p. 2, 2026. doi:10.1007/s41365-025-01855-5

[10] X. Deng, Z. Pan, J. Zhao, Z. Li, A. Chao, and C. Tang, "Reversible microbunching in an electron storage ring", submitted for publication.

[11] G. Stupakov, "Using the beam-echo effect for generation of short-wavelength radiation", *Phys. Rev. Lett.*, vol. 102, p. 074801, 2009. doi:10.1103/PhysRevLett.102.074801

[12] Z. Pan, J. Zhao, C. Tang, X. Deng, and A. Chao, "Isochronous lattice design with time-of-flight fluctuation reaching subattoseconds based on high order achromat", *Phys. Rev. Accel. Beams*, vol. 28, p. 124001, 2025. doi:10.1103/3v8n-84fr

[13] Z. Pan, W. Wu, J. Zhao, X. Deng, A. Chao, and C. Tang, "The accurate calculation for intra-beam scattering induced path length deviation of an electron beam traveling the lattice", submitted for publication.

[14] K. Kubo and K. Oide, "Intrabeam scattering in electron storage rings", *Phys. Rev. ST Accel. Beams*, vol. 4, p. 124401, 2001. doi:10.1103/PhysRevSTAB.4.124401

[15] M. Borland, "Elegant: a flexible SDDS-compliant code for accelerator simulation", Argonne National Lab., Argonne, IL, USA, Rep. LS-287, 2000.